

Article

# Changes in a Giant Iceberg Created from the Collapse of the Larsen C Ice Shelf, Antarctic Peninsula, Derived from Sentinel-1 and CryoSat-2 Data

Hyangsun Han <sup>1,\*</sup>, Sungjae Lee <sup>1</sup>, Jae-In Kim <sup>1</sup>, Seung Hee Kim <sup>1</sup> and Hyun-cheol Kim <sup>1</sup>

Unit of Arctic Sea-Ice Prediction, Korea Polar Research Institute (KOPRI), Incheon 21990, Korea; sungjae@kopri.re.kr (S.L.); jikim0312@kopri.re.kr (J.-I.K.); seunghee@kopri.re.kr (S.H.K.); kimhc@kopri.re.kr (H.-c.K.)

\* Correspondence: hyangsun@kopri.re.kr; Tel.: +82-32-760-5811

Received: 31 December 2018; Accepted: 14 February 2019; Published: 17 February 2019



**Abstract:** The giant tabular iceberg A68 broke away from the Larsen C Ice Shelf, Antarctic Peninsula, in July 2017. The evolution of A68 would have been affected by both the Larsen C Ice Shelf, the surrounding sea ice, and the nearby shallow seafloor. In this study, we analyze the initial evolution of iceberg A68A—the largest originating from A68—in terms of changes in its area, drift speed, rotation, and freeboard using Sentinel-1 synthetic aperture radar (SAR) images and CryoSat-2 SAR/Interferometric Radar Altimeter observations. The area of iceberg A68A sharply decreased in mid-August 2017 and mid-May 2018 via large calving events. In September 2018, its surface area increased, possibly due to its longitudinal stretching by melting of surrounding sea ice. The decrease in the area of A68A was only 2% over 1.5 years. A68A was relatively stationary until mid-July 2018, while it was surrounded by the Larsen C Ice Shelf front and a high concentration of sea ice, and when its movement was interrupted by the shallow seabed. The iceberg passed through a bay-shaped region in front of the Larsen C Ice Shelf after July 2018, showing a nearly circular motion with higher speed and greater rotation. Drift was mainly inherited from its rotation, because it was still located near the Bawden Ice Rise and could not pass through by the shallow seabed. The freeboard of iceberg A68A decreased at an average rate of  $-0.80 \pm 0.29$  m/year during February–November 2018, which could have been due to basal melting by warm seawater in the Antarctic summer and increasing relative velocity of iceberg and ocean currents in the winter of that year. The freeboard of the iceberg measured using CryoSat-2 could represent the returned signal from the snow surface on the iceberg. Based on this, the average rate of thickness change was estimated at  $-12.89 \pm 3.34$  m/year during the study period considering an average rate of snow accumulation of  $0.82 \pm 0.06$  m/year predicted by reanalysis data from the Modern-Era Retrospective analysis for Research and Applications, version 2 (MERRA-2). The results of this study reveal the initial evolution mechanism of iceberg A68A, which cannot yet drift freely due to the surrounding terrain and sea ice.

**Keywords:** iceberg A68A; Larsen C Ice Shelf; Antarctic Peninsula; Sentinel-1; CryoSat-2; MERRA-2

## 1. Introduction

An iceberg is a freely floating mass of ice calved from a glacier, ice shelf, or larger iceberg. Many icebergs exist around Antarctica and they travel the Southern Ocean via ocean currents and atmospheric winds [1–3]. Monitoring of the icebergs is very important because their evolution can produce fresh meltwater into the ocean, which has a profound impact on sea ice formation [4,5], ocean circulation [1,6], marine ecosystems [7–9], and ship navigation [10]. Moreover, the evolutionary processes of icebergs can be key to finding causes of the on-going decay of the Antarctic ice shelves with the ocean and sea level change [11].

Satellite radar remote sensing is useful for monitoring icebergs, because it can observe the Earth's surface regardless of weather conditions and sun altitude. The Brigham Young University and National Ice Center (NIC) have constructed a comprehensive database for Antarctic iceberg tracking, by analyzing microwave scatterometer data, and provide information about the locations and rotations of icebergs [12]. Satellite microwave scatterometers can observe the whole of Antarctica daily, but the spatial resolution of data generated is several tens of kilometers [12,13], which is not enough to observe changes in icebergs in detail. Using synthetic aperture radar (SAR), which provides higher spatial resolution data, a detailed analysis of even small changes in icebergs is possible. Many studies have used SAR to monitor changes in Antarctic icebergs [14–18]. For example, Moctezuma-Flores and Parimiggiani [16] analyzed the drift characteristics of iceberg C33 calved from the Nansen Ice Shelf, East Antarctica, using Sentinel-1 SAR images shortly after the ice shelf collapsed. Li et al. [17] observed the evolution of the tabular icebergs C28A and C28B between 2010 and 2012 using ENVISAT Advanced Synthetic Aperture Radar (ASAR) images, which originated from the Mertz Ice Tongue in East Antarctica.

Satellite altimeters are necessary to analyze iceberg thinning. The radar altimeter (RA) is more useful than the laser altimeter in polar regions due to frequent cloudy weather. CryoSat-2 SAR/Interferometric Radar Altimeter (SIRAL) is more useful for observing iceberg freeboard change than previous generation RAs such as the RA on board ERS-1/2 and the RA-2 on board ENVISAT. This is because it can estimate ice topography with higher accuracy and higher spatial resolution [19]. In recent research on icebergs C28A and C28B [17], CryoSat-2 data were very helpful for analyzing freeboard change.

In July 2017, a supersized iceberg broken away from the Larsen C Ice Shelf in the Antarctic Peninsula, named A68 by the NIC. The initial area of the A68 was about 5800 km<sup>2</sup> when it calved [20], which accounts for approximately 10% of the Larsen C Ice Shelf [21,22]. Based on the iceberg tracking database operated by the Brigham Young University and NIC, iceberg A68 is currently the largest iceberg in Antarctica and the sixth largest on satellite observation records. Iceberg A68 is surrounded by dense sea ice throughout the year and the nearby seabed is shallow [23]. This means that it is expected to show complex evolution, different from freely moving icebergs. Although the evolution of iceberg A68 could have a significant impact on the marine environment around the Antarctic Peninsula, few studies on iceberg A68 have been conducted so far. There is one study on the changes in area and drift of the iceberg based on SAR image analysis [18], observing the changes for only six months after the iceberg formation. Moreover, the environmental factors affecting the changes of iceberg have not been analyzed.

The objectives of this study are to (1) analyze the initial evolution of iceberg A68 in terms of changes in its area, drift speed, rotation, and freeboard over the 1.5-year period since it calved from the Larsen C Ice Shelf using Sentinel-1 SAR and CryoSat-2 SIRAL observations and (2) investigate the effects of environmental factors on these changes. Descriptions of the iceberg and the dataset used in this research are presented in Section 2. Section 3 explains the methods adopted for deriving information about the iceberg's evolution from satellite data. Section 4 provides a discussion of the results and the observed iceberg changes, and Section 5 provides a conclusion.

## 2. Materials

### 2.1. Iceberg A68

A crack on the Larsen C Ice Shelf, the largest ice shelf on the Antarctic Peninsula, formed near the Gipps Ice Rise over a decade ago and started to propagate across the ice shelf in 2014 [21,22]. The crack joined-up with several others as it advanced northward, and finally formed a giant tabular iceberg (A68) in July 2017 (Figure 1). Iceberg A68 had a length of 160 km and width of 50 km when it was released from the ice shelf. The thickness and weight of the iceberg was presumed to be approximately 300 m and 1 trillion tons, respectively [20]. Shortly after A68 separated from the Larsen C Ice Shelf, it

split into two major pieces—A68A and A68B. Iceberg A68B is the smaller of the two, with an area of 90 km<sup>2</sup>, and accounts for only 2% of the total area of A68 (Figure 1). In this study, we focus on iceberg A68A. Iceberg A68A is expected to show complex dynamics as it is surrounded by the Larsen C Ice Shelf at its back and by highly concentrated sea ice in front. Moreover, the seabed elevations (elevation below sea level) near Bawden and Gipps Ice Rises, located at the north and south of the iceberg, are higher than −300 m (Figure 1), which might interfere with the drift of A68A.

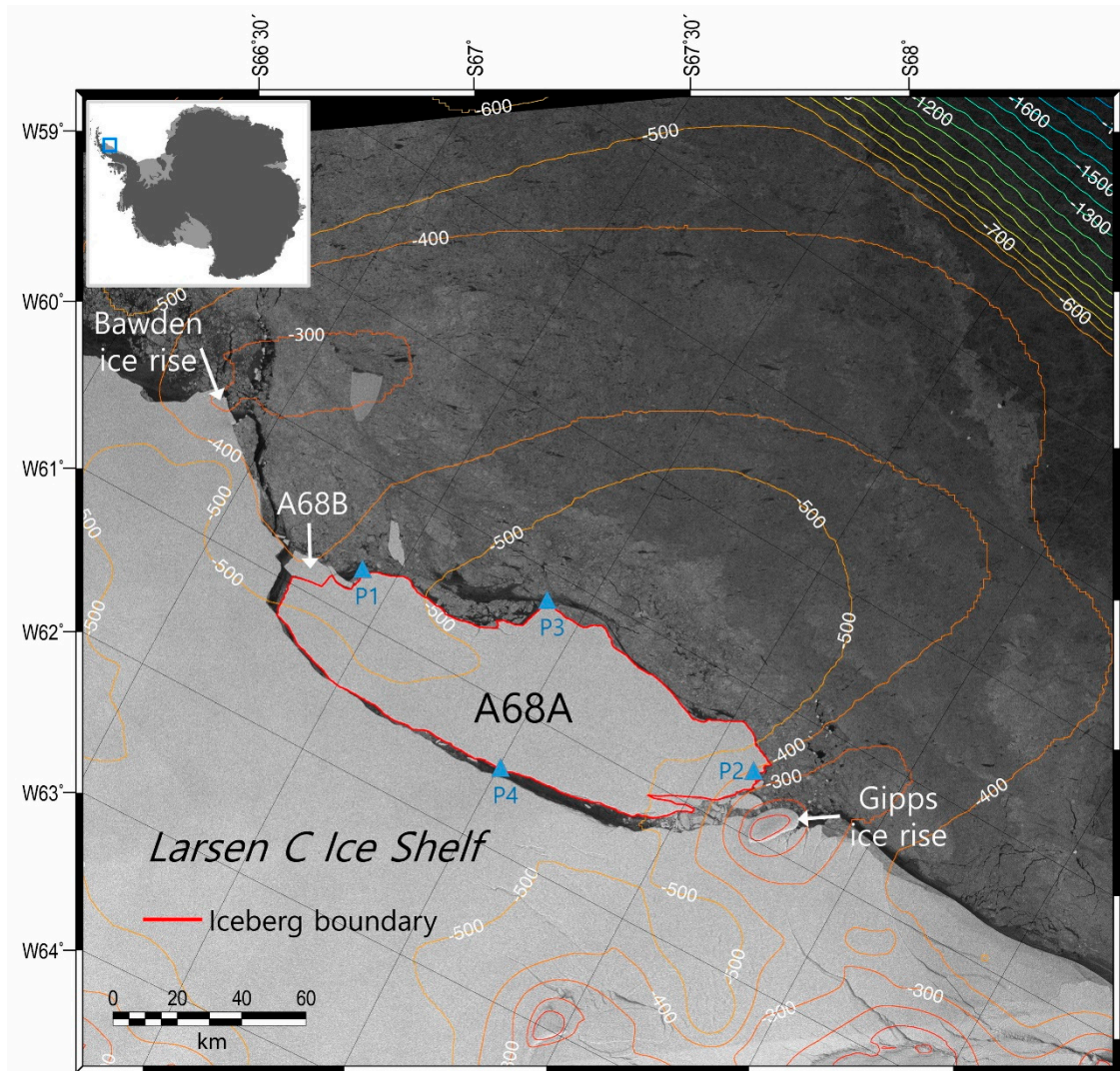


**Figure 1.** Sentinel-1A synthetic aperture radar (SAR) image for the study area (rectangle in the inset) obtained on 28 July 2017 overlaid with contour of seafloor from Bedmap2 in the polar stereographic projection. Points P1, P2, P3, and P4 on the edges of the iceberg have hardly show any calving. Drift speed and rotation of the iceberg were calculated at P1 and P2. The stretching rates of the iceberg were measured along the straight lines connecting the points P1 and P2, and P3 and P4, respectively.

## 2.2. Data

A total of 78 Sentinel-1 SAR images were obtained for A68A from 22 July 2017 to 29 November 2018, which were used to estimate area and drift. The two Sentinel-1 constellation satellites (Sentinel-1A and 1B) are equipped with C-band SAR with a center frequency of 5.405 GHz [24]. Each satellite has a temporal resolution of 12 days, while the satellite constellation follows the same ground track and can thus provide images for the same area every six days. All Sentinel-1 SAR images were obtained with HH-polarization in the Extra Wide swath mode, which captures an area of  $400 \times 400$  km with a spatial resolution of  $20 \times 40$  m (range  $\times$  azimuth).

CryoSat-2 SIRAL (Ku-band RA with a center frequency of 13.575 GHz) surface elevation profiles were used to estimate the freeboard of iceberg A68A. The repeat cycle of CryoSat-2 is 369 days with a 30-day sub-cycle [19]. The along-track spacing of CryoSat-2 is approximately 350 m and the across-track spacing is less than 2.5 km, at 70 S, with footprint of roughly 300 m and 1.5 km, respectively [19,25], which provides high-density data for estimating freeboard. Over the margins of ice sheets and mountain glaciers, CryoSat-2 is operating in SAR Interferometric (SARIn) mode, which provides more accurate topography information in steep areas than previously operated RA systems [19,25,26]. The CryoSat-2 level 2 Baseline C data in SARIn mode were used, which covered iceberg A68A during the Sentinel-1 SAR observation period. We used the EIGEN-6C4 Geoid [27], DTU12MDT mean dynamic topography [28], and Circum-Antarctic Tidal Simulation Inverse tide model version 2008 (CATS2008a) [29] to correct the freeboard of the iceberg, converted from the ellipsoidal iceberg surface elevation provided by the CryoSat-2 Level 2 data.

The 10-m air temperature, 10-m wind speed, and snow depth around A68A were predicted from Modern-Era Retrospective analysis for Research and Applications, version 2 (MERRA-2) reanalysis data [30], using a grid size resolution of  $0.5^\circ \times 0.625^\circ$  (latitude  $\times$  longitude) to analyze the effects of environmental factors on iceberg changes. MERRA-2 has the latest atmospheric reanalysis data produced by NASA's Global Modeling and Assimilation Office (GMAO), which provides a long-term record of global atmosphere since 1980. Air temperature and wind speed can affect iceberg area and drift, respectively. Snow depth was considered in the analysis of iceberg freeboard change assuming CryoSat-2 Ku-band SIRAL might not penetrate snow cover on the iceberg A68A owing to high firm densification which is causative of low penetration depth of the radar signal [19].

To investigate the relationship between iceberg evolution and submarine topography, seabed elevation data from Bedmap2 [31] were used with a 1-km grid size. Bedmap2 incorporates a number of Antarctic sub-ice shelf and deep ocean bathymetry datasets provided by British Antarctic Survey.

## 3. Methods

The area of iceberg A68A was measured by delineating its boundary from the Sentinel-1 SAR images. The boundary of iceberg can be automatically delineated from SAR image by using well-known edge filters or object-based iceberg detection methods [15,18,32]. However, the automatic detection techniques might produce incorrect result when there is low brightness contrast between the iceberg and the surroundings [15]. In several Sentinel-1 SAR images obtained in summer, iceberg A68A appeared as dark as the surrounding sea ice due to snowfall or ice surface melting (see Figure 4b) and would not be delineated correctly by the automatic detection techniques. For these reasons, the area of iceberg A68A was extracted by carefully digitizing the boundary of the iceberg captured in the Sentinel-1A/B SAR images based on visual inspection. The uncertainty in the iceberg area was calculated as the standard deviation of the area derived from repeatedly digitizing the same image by a single operator [33]. The drift speed and rotation angle of the iceberg were calculated by measuring the locations of the iceberg in consecutive SAR images. We calculated drift speed and rotation angle at the center of the iceberg, and points on the northern and southern edges of the iceberg (P1 and P2 in Figure 1) where there have hardly been any collapses so far. The locations of P3 and P4 have also hardly calved during the observation period. The changes in lengths of P1–P2 and P3–P4 with respect to time were calculated to analyze the stretching of the iceberg.

The freeboards of A68A were derived from the CryoSat-2 profiles inside the boundary of the iceberg identified from the Sentinel-1 SAR images acquired on the same dates. The time difference of a few hours between the CryoSat-2 and Sentinel-1 observations was disregarded as the iceberg moves less than 100 meters per hour (see Section 4). To correct for the potential errors in the ellipsoidal surface elevation of A68A as measured by the CryoSat-2, we applied the freeboard measurements method described in [25]. For this, the ellipsoidal iceberg surface elevation was converted to the freeboard value using EIGEN-6C4 Geoid, in which changes in sea surface height by non-tidal and tidal effects are corrected using the DTU12MDT and CATS2008a models, respectively. The freeboard of the iceberg A68A was derived from CryoSat-2 observations assuming that the iceberg is in the hydrostatic equilibrium state.

The CryoSat-2 freeboard profile on 8 September 2017 was plotted over the Sentinel-1A SAR image acquired on the same date (Figure 2). Other CryoSat-2 profiles acquired on different dates were relocated to the location of A68A on 8 September 2017 based on the drift speed and rotation angle of the iceberg (Figure 2). The freeboard changes were calculated at the intersections of the CryoSat-2 profiles, with a total time span of more than 180 days. We derived the linear fitting of each freeboard profile using the least squares method to define the intersections of different profiles. The mean and standard deviation of freeboard values for each profile located within a radius of 1.5 km from the point of the intersection were used to calculate freeboard change. Averaging the freeboard values within the 1.5 km radius can reduce systematic errors in the CryoSat-2 observations, and the calculated standard deviations can be regarded as a measure of freeboard uncertainty [17].

If the iceberg is in a hydrostatic equilibrium state, the change in ice thickness ( $\Delta Z$ ) can be estimated by [34]

$$\Delta Z = \frac{\rho_w}{\rho_w - \rho_i} \Delta e - \frac{\rho_w - \rho_s}{\rho_w - \rho_i} \Delta \delta \quad (1)$$

where  $\Delta e$  is the change in freeboard,  $\Delta \delta$  is the change in snow depth and firn densification,  $\rho_i$  is the ice density,  $\rho_w$  is the sea water density, and  $\rho_s$  is the snow/firn density, respectively [25,34]. The density of ice and sea water has been assumed as 917 kg/m<sup>3</sup> and 1027–1030 kg/m<sup>3</sup>, respectively, in many studies on thickness estimation of the Antarctic ice shelves from the freeboard measurements by satellite altimetry [25,35–38]. We used 917 kg/m<sup>3</sup> and 1027 kg/m<sup>3</sup> as the density of ice and water. Snow density of 300 kg/m<sup>3</sup> [34] was used in this study. The change in firn densification should also be considered in the estimation of iceberg thickness change from the freeboards. However, snow depth predicted by MERRA-2 used in this study does not fully reflect the firn densification and there is no information about changes in firn densification of iceberg A68A. Nevertheless, we estimated the changes in thickness of iceberg A68A, ignoring the changes in firn densification. This is because the change in firn densification around the West Antarctic ice shelves is approximately only −2.7 cm/year [39] which is significantly smaller than the freeboard changes in iceberg A68A (see Section 4). The volume loss of iceberg A68A caused by the thickness changes was also analyzed in this study.

Changes in the area, drift speed, rotation angle, and freeboard of iceberg A68A were analyzed with the environmental factors predicted from the MERRA-2 reanalysis fields and seabed topography from Bedmap2. This enabled us to assess the possible causes of iceberg evolution.

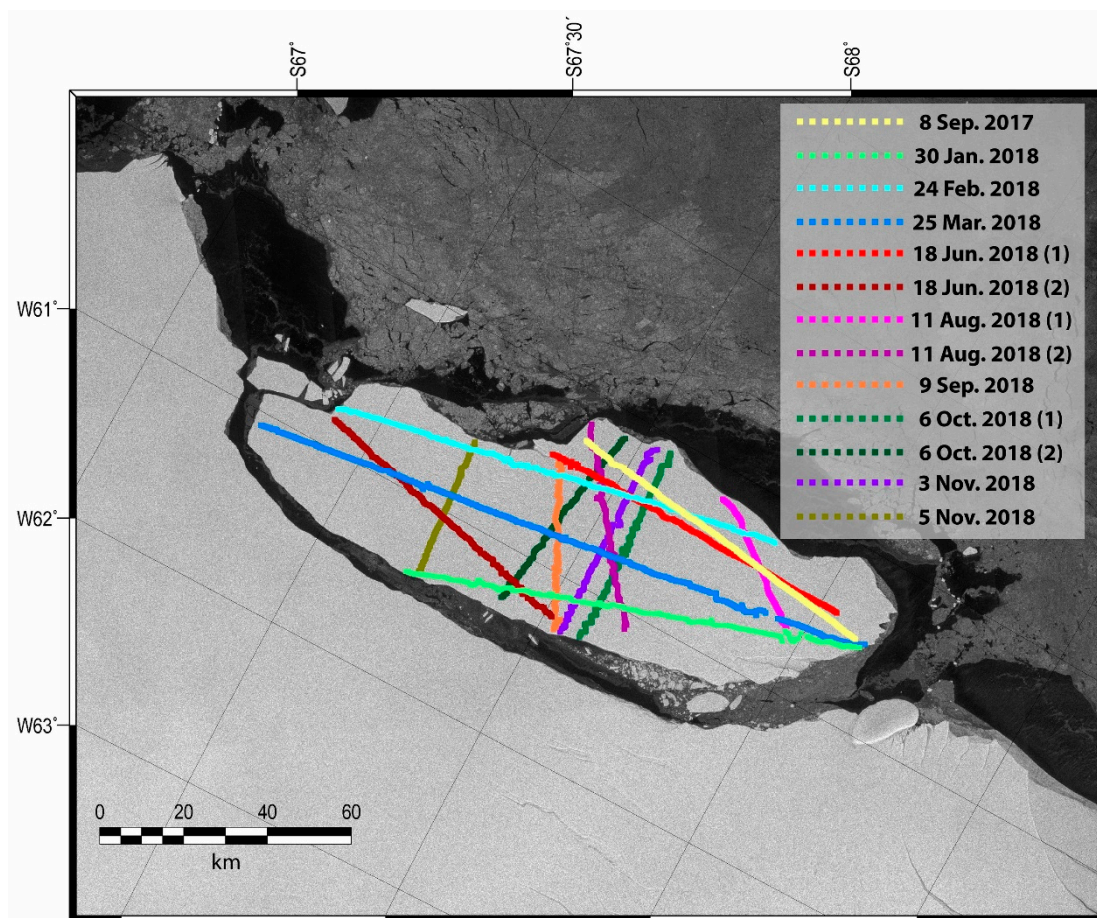


**Figure 2.** CryoSat-2 SAR Interferometric (SARIn) mode profiles on iceberg A68A overlaid on the Sentinel-1A SAR image acquired on 8 September 2017. The freeboard changes of the iceberg were calculated at the intersections of the different profiles which have a time difference of more than 180 days.

#### 4. Results and Discussion

The area of iceberg A68A was 5786.3 km<sup>2</sup> when it was initially formed (Figures 1 and 3a). Its area decreased by 35 km<sup>2</sup> in mid-August 2017, when ice pieces broke away (Figure 4a), and then remained almost constant until mid-May 2018. In mid-May 2018, another large ice chunk calved (Figure 4c) and the area of A68A dramatically decreased to 5620 km<sup>2</sup>. There was little subsequent change in the area of the iceberg until September 2018 in which the area slightly increased by approximately 30 km<sup>2</sup>. Large ice chunks were concentrated on the northern part of the iceberg, with little separation of debris in other parts (Figure 4a,c). Calving occurs by the extension of cracks on the top and bottom surfaces of icebergs, which can be caused by increases in air and sea surface temperatures, wind, and current drag forces, and via interaction with the surrounding topography [17,40]. However, the observed trends in air temperature predicted by the MERRA-2 reanalysis data did not match changes in iceberg area (Figure 3a). As A68A was surrounded by sea ice throughout the observation period, we did not compare changes in iceberg area with sea surface temperature. In August 2017 and May 2018, when the large ice chunks calved from A68A, southerly winds blew at 6–12 m/s (Figure 5), which were strong enough to move the iceberg north and to break the surrounding packed sea ice [41]. However, the iceberg hardly moved as the iceberg collided with the coastline of the Larsen C Ice Shelf and the shallow seabed near the Bawden Ice Rise (Figure 1). This created ice fragments in the northern part of the iceberg via crack extension on the top and bottom surfaces.

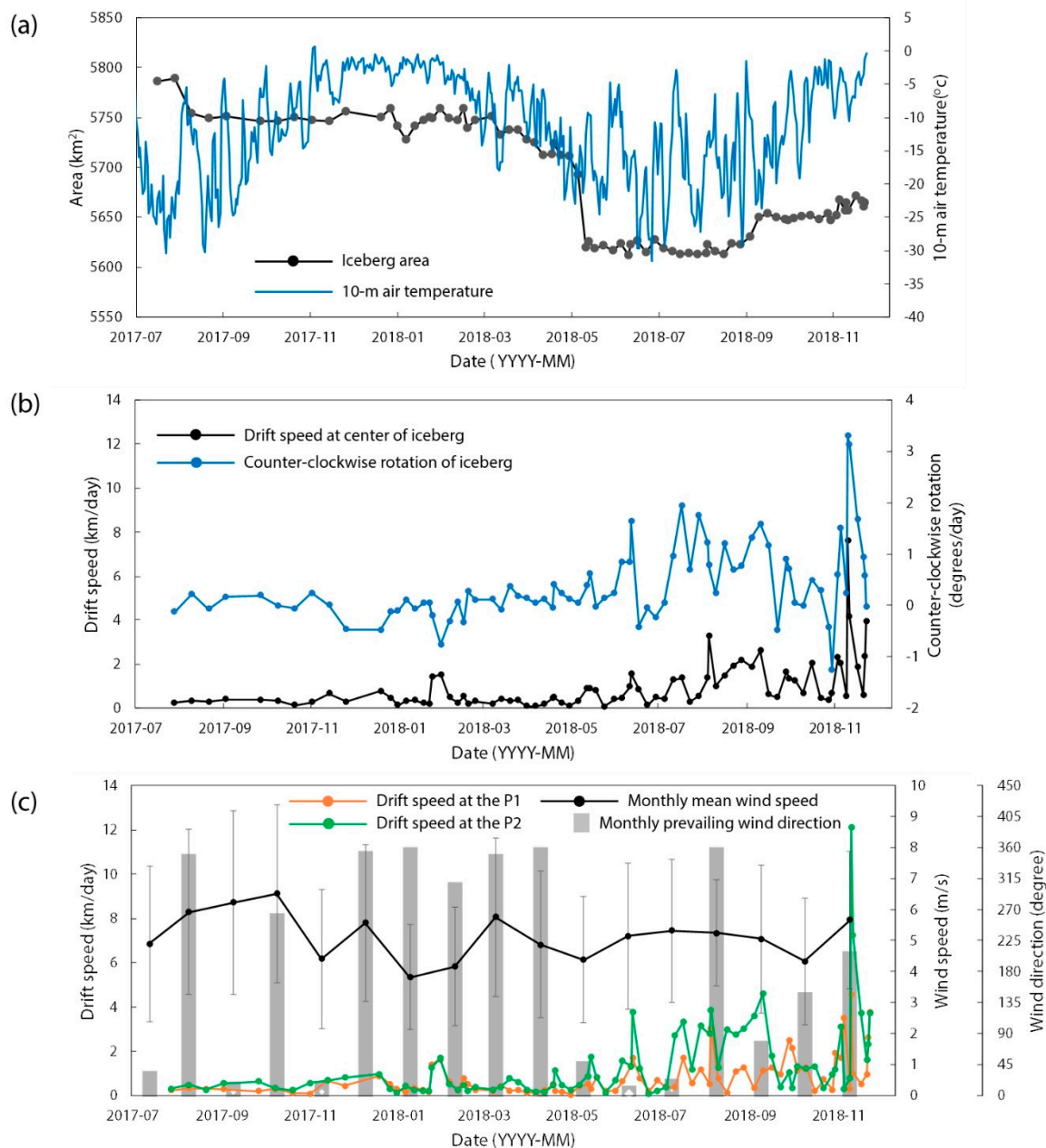


**Figure 3.** (a) Changes in the area of iceberg A68A and 10-m air temperature around the iceberg predicted by the Modern-Era Retrospective analysis for Research and Applications, version 2 (MERRA-2); (b) Changes in the drift speed at the center of iceberg A68A and its rotation angle; (c) Changes in the drift speed at the location of P1 and P2 of iceberg A68A, and monthly mean wind speed and prevailing wind direction ( $0^\circ$  = from south,  $90^\circ$  = from west,  $180^\circ$  = from north,  $270^\circ$  = from east) around the iceberg predicted by the MERRA-2. The vertical error bars in (c) represent the standard deviation of wind speeds for each month.

It is worth noting that the increase in iceberg area was measured in September 2018. This was likely caused by error in the visual digitization of SAR images or by an actual increase in surface area due to the longitudinal stretching of the iceberg. The digitizing errors calculated as the standard deviations of the repeatedly measured iceberg areas from the same images through visual inspection were small, ranging from 2.7 to 7.8 km<sup>2</sup>. There were no significant calving events after mid-May 2018. Longitudinal stretching of ice mass is possible if external restraining forces on its boundaries are small or not present [42,43]. Ice shelves experience similar longitudinal stretching and thinning

when they lose buttressing forces due to unpinning or iceberg calving [44]. The observation of A68A shows that the sea ice in the northwestern region of A68A started to disappear since July 2018 (Figure 4). We suspect that this reduced the external restraining forces on the iceberg and caused longitudinal stretching in the horizontal direction. The horizontal stretching can occur around the iceberg. We measured the stretching rate along the straight line connecting the points P1 and P2, and P3 and P4 from the six SAR images in Figure 4. The stretching rates were smaller than 0.008/year before July 2018 (Figure 4b–d). However, the rates increased sharply from July to September 2018, showing the value of 0.013 /year and 0.026 /year along the line P1–P2 and P3–P4, respectively (Figure 4e). This suggests that the measured increase resulted from an increase in the area of the iceberg due to the longitudinal stretching after August 2018. The area of A68A at the end of November 2018 was 5660.1 km<sup>2</sup>, which was just 2% less than at the time of its formation.

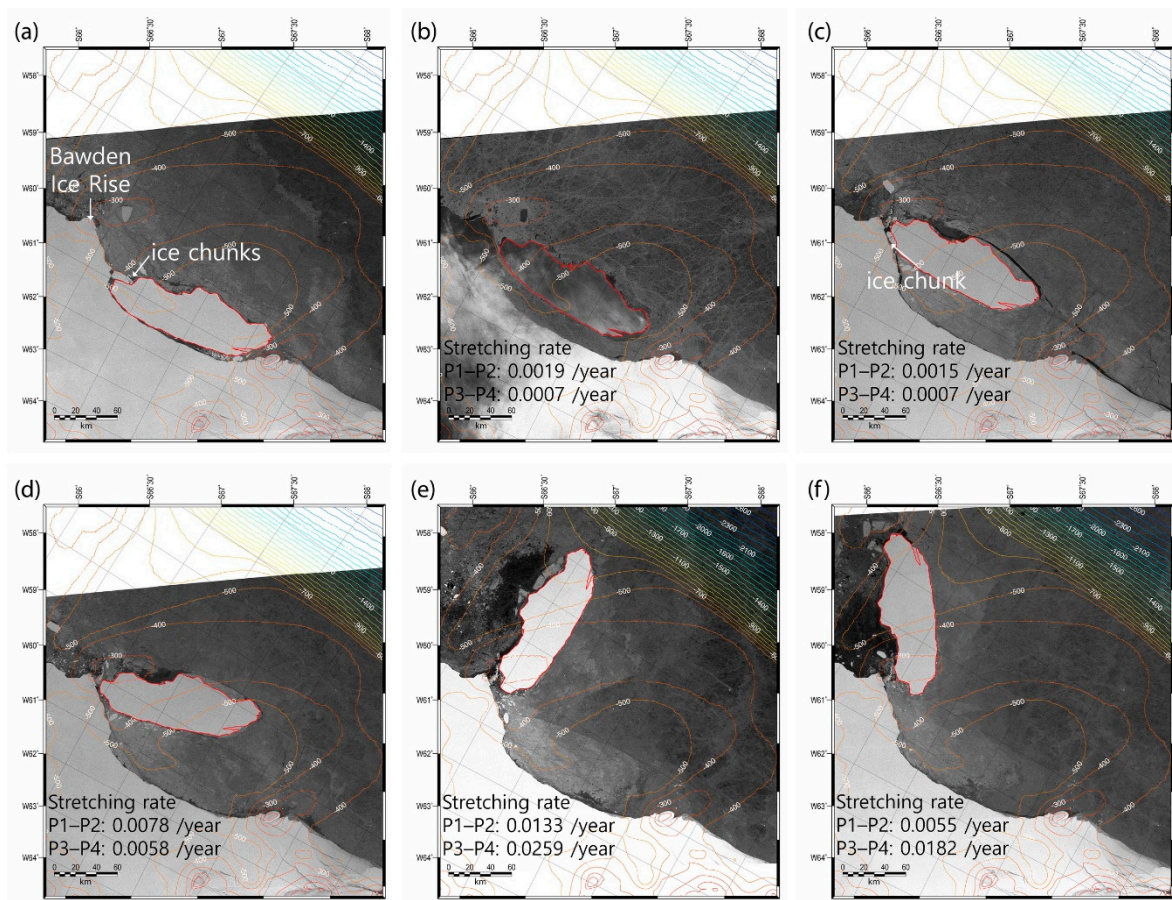


**Figure 4.** The Sentinel-1 SAR images of iceberg A68A acquired on (a) 15 August 2017; (b) 12 January 2018; (c) 18 May 2018; (d) 17 July 2018; (e) 16 September 2018; and (f) 27 November 2018.

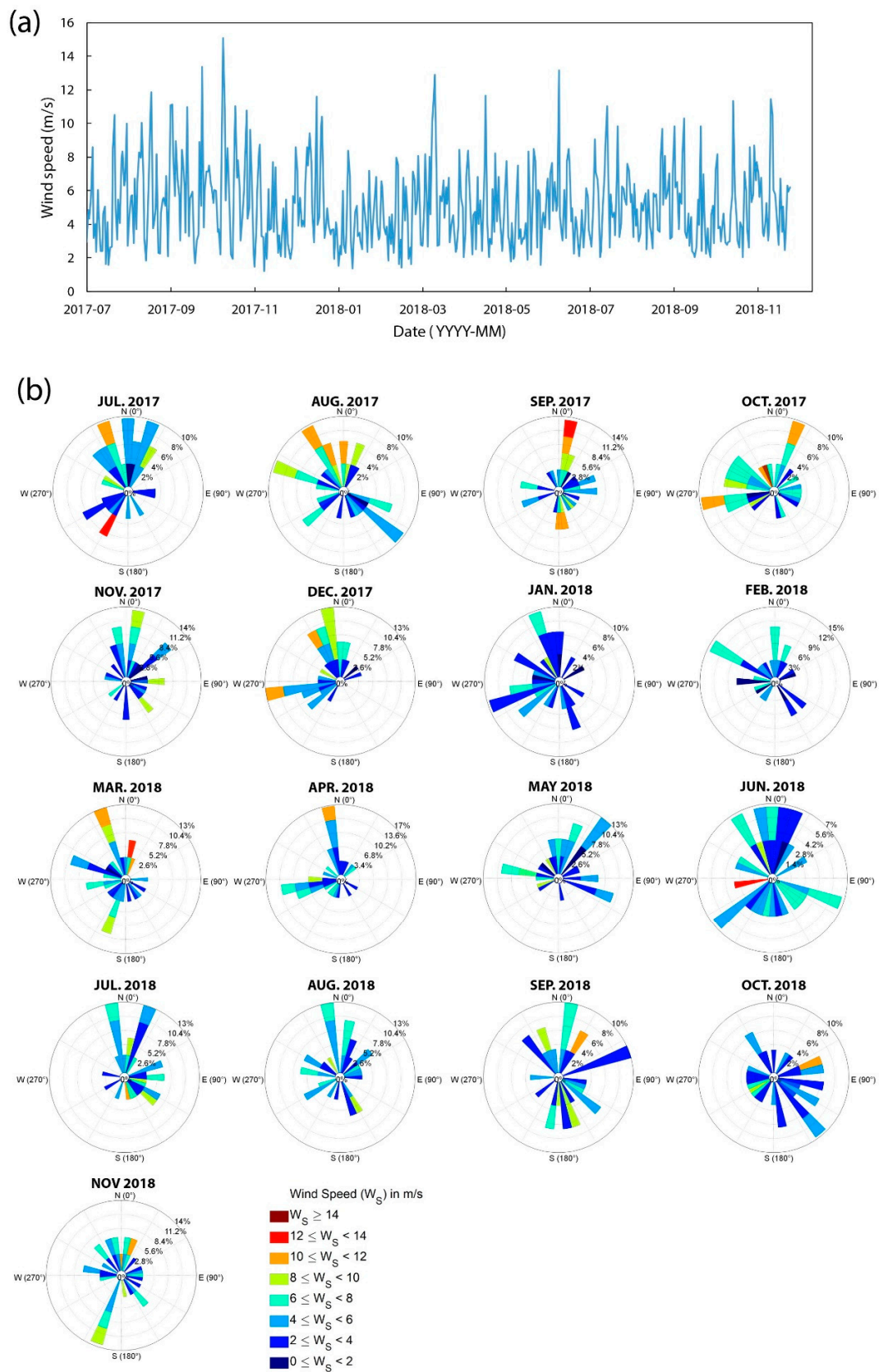


**Figure 5.** (a) Changes in the wind speed around iceberg A68A predicted by the MERRA-2; (b) Wind rose showing wind speed and direction for each month during July 2017–November 2018.

Prior to mid-July 2018, drift speed at the center of iceberg and rotation angle were generally less than 2 km/day and  $\pm 1^\circ$ /day (the positive value of rotation angle indicates a counter-clockwise rotation), respectively (Figure 3b). The northern and southern part of the iceberg (the location of P1 and P2, respectively, in Figure 1) also showed very low drift speed before mid-July 2018 (Figure 3c). This was driven by strong easterly and southerly winds (Figure 5b), the high concentration of sea ice and the front of the Larsen C Ice Shelf that limited the movement and rotation of A68A. During July 2017–August 2018, the prevailing wind directions were the north and the mean wind speeds were 4–7 m/s (Figure 3c). The iceberg gradually moved northward due to southerly winds and finally emerged from the front of Larsen C Ice Shelf in July 2018 (Figure 4d). Iceberg A68A moved faster after mid-July 2018, especially in the southern part of the iceberg (Figure 3b,c), and showed nearly circular motion. A68A escaped from the bay-shaped region, but the northern part of the iceberg remains near to the Bawden Ice Rise (Figure 4e–f). Therefore, rotation in a counter-clockwise direction has only occurred (Figure 3b) even though westerly winds were becoming more and more frequent (Figures 3c and 5b).

As outlined above, the movement of iceberg A68A was likely interrupted by the shallow seabed, specifically nearby the Bawden Ice Rise. The assumption of hydrostatic equilibrium cannot be valid when the iceberg is pinned to the shallow seabed. However, movement of the iceberg was only limited by the ice rise and it continued to drift. Therefore, we assumed that the ice rise had only a small effect on the hydrostatic equilibrium state of the iceberg.

Freeboard changes for A68A derived from the CryoSat-2 observations are shown in Table 1. Most of the freeboard change values calculated using the CryoSat-2 observations on 8 September 2017 and 30 January 2018 as a reference (intersections 1–9 in Table 1) were positive, with an averaging change of  $0.82 \pm 0.38$  m/year. Calculated freeboard changes after February 2018 (intersections 10–18 in Table 1) were mostly negative, however, with an averaging change of  $-0.80 \pm 0.29$  m/year. A positive value indicates that the freeboard is rising during the observation period, i.e., ice thickening is occurring. As an iceberg is completely detached from the grounded ice sheet and ice shelf, its thickness naturally decreases due to basal melting and surface sublimation/ablation [17,45,46]. CryoSat-2 SIRAL uses the Ku-band that might measure the maximum return from the snow surface on the iceberg A68A due to high densification of snow/firn layer [19]. Figure 6 shows the increase in snow depth for a region of the Larsen C Ice Shelf near iceberg A68A, as predicted by the MERRA-2 reanalysis data. The snow depth in this region continued to increase during the entire observation period, except for January–February 2018 when a small reduction was observed. The linear fitting of the changes in snow depth shows that the rate of increase rate was  $0.82 \pm 0.06$  m/year. Therefore, the increase in the freeboard of iceberg A68A (using the 8 September 2017 and 30 January 2018 reference values) was likely the result of increased snow depth on the ice surface and not ice thickening, and the thickness of the iceberg possibly remained constant until January 2018.

The decrease in the freeboard of A68A after February 2018 indicates that the iceberg thinning rate was greater than the rate of snow depth increase. In other words, the thickness of A68A has decreased dramatically since February 2018. This likely reflects warm seawater during the Antarctic summer, and an increase in the relative velocity of the iceberg resulting from drift in winter (Figure 3b) promoted the basal melting [17,45]. The longitudinal stretching of the iceberg after August 2018 could also contribute to the decrease in the freeboard as it is accompanied by ice thinning [44]. Assuming that CryoSat-2 observations reflect the maximum radar returns from the snow surface on the iceberg, the averaging rate of thickness change during February–November 2018 was calculated as  $-12.89 \pm 3.34$  m/year from Equation (1) based on an averaging snow depth change of  $0.82 \pm 0.06$  m/year. The thickness changes of the iceberg could be influenced by the changes in firn densification and basal melting. The effect of the changes in firn densification on the freeboard change is much smaller than basal melting of iceberg [45]. Zwally et al. [39] showed that the change in firn compaction in the West Antarctic ice shelves is  $-2.7$  cm/year. Therefore, the thinning of iceberg A68A was mainly attributed to basal melting. Assuming that the ice thinning rate and thickness (300 m from Bedmap2) were constant

over the whole iceberg, the volume loss of the iceberg caused by both calving and basal melting was approximately  $1.12 \times 10^5$  tons.

**Table 1.** The freeboards of iceberg A68A at the intersections of different CryoSat-2 profiles shown in Figure 2.

No. Intersections	Date	Freeboard (m)	No. Intersections	Dates	Freeboard (m)
1	2017.09.08	$34.5 \pm 0.2$	10	2018.02.24	$34.6 \pm 0.4$
	2018.06.18 (1)	$36.1 \pm 0.1$		2018.09.09	$32.7 \pm 0.7$
2	2017.09.08	$34.4 \pm 0.2$	11	2018.02.24	$36.1 \pm 0.6$
	2018.08.11 (1)	$35.3 \pm 0.2$		2018.10.06 (1)	$36.1 \pm 0.2$
3	2017.09.08	$35.1 \pm 0.2$	12	2018.02.24	$34.5 \pm 0.9$
	2018.10.06 (1)	$35.7 \pm 0.2$		2018.10.06 (2)	$33.0 \pm 0.3$
4	2017.09.08	$32.7 \pm 1.2$	13	2018.02.24	$36.5 \pm 0.2$
	2018.10.06 (2)	$31.9 \pm 0.4$		2018.11.03	$35.9 \pm 0.3$
5	2017.09.08	$35.1 \pm 0.3$	14	2018.02.24	$33.5 \pm 0.6$
	2018.11.03	$35.3 \pm 0.1$		2018.11.05	$33.0 \pm 0.5$
6	2018.01.30	$35.7 \pm 0.6$	15	2018.03.25	$36.4 \pm 0.5$
	2018.08.11 (2)	$36.7 \pm 0.5$		2018.10.06 (1)	$37.0 \pm 0.8$
7	2018.01.30	$37.8 \pm 1.9$	16	2018.03.25	$35.8 \pm 0.7$
	2018.09.09	$38.6 \pm 0.7$		2018.10.06 (2)	$36.1 \pm 0.4$
8	2018.01.30	$37.0 \pm 2.1$	17	2018.03.25	$38.0 \pm 0.3$
	2018.10.06 (1)	$37.5 \pm 1.1$		2018.11.03	$37.9 \pm 0.2$
9	2018.01.30	$38.7 \pm 0.6$	18	2018.03.25	$36.0 \pm 0.2$
	2018.11.03	$39.0 \pm 0.4$		2018.11.05	$35.1 \pm 0.4$

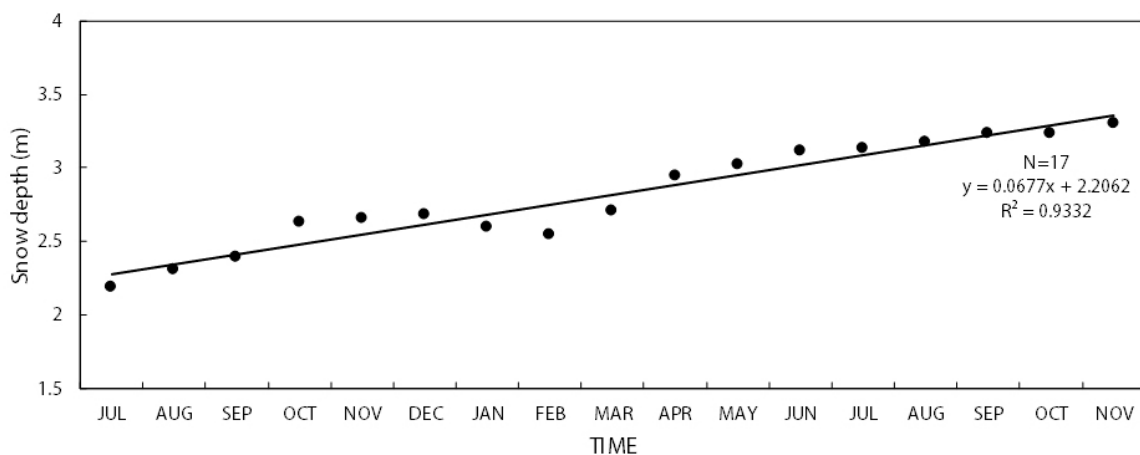


**Figure 6.** Monthly averaged snow depth on glaciated area around iceberg A68A predicted by the MERRA-2. N is the number of data points.

According to the Sentinel-1 observations, A68A was still located near the Bawden Ice Rise as of the end of November 2018, and it is rotating without significant movement (Figure 4). This is probably because the western part of the iceberg is not free to move past the ice rise. It is not easy to predict when A68A will drift away from the ice rise. However, as summer approaches, its rate of thinning will increase, which will make the ice rise less effective. A68A might also move further out to ocean when strong westerly winds blow, after which it will drift at a much faster rate, and its area and thickness will decrease more rapidly.

Although we observed changes over a period of only 1.5 years, the initial evolution of iceberg A68A could be analyzed, characterized by drift that was limited by complex terrain and the surrounding sea ice.

## 5. Conclusions

The evolution of iceberg A68A, a giant tabular iceberg calved from the Larsen C Ice Shelf in July 2017, was analyzed in terms of area, drift speed, rotation, and freeboard using Sentinel-1 SAR images, CryoSat-2 profiles, and environmental factors predicted by the MERRA-2 reanalysis data. The iceberg showed little change in area over time, except in mid-August 2017 and mid-May 2018 when it decreased sharply due to ice calving, and in September 2018 when it increased possibly due to its longitudinal stretching by melting of surrounding sea ice. Air temperature trends had little effect on iceberg area. At the end of November 2018, the iceberg area (5660.1 km<sup>2</sup>) was just 2% less than at the time of formation (5786.3 km<sup>2</sup>). The drift speed and rotation of the iceberg prior to mid-July 2018 were very small due to the drift being interrupted by the Larsen C Ice Shelf, a high concentration of surrounding sea ice, and a shallow seabed. The iceberg escaped from the bay-shaped region in front of the Larsen C Ice Shelf in mid-July 2018, but only rotated without significant movement due to the shallow seabed near the Bawden Ice Rise. The iceberg freeboard measured using CryoSat-2 observations has dramatically decreased since February 2018 ( $-0.80 \pm 0.29$  m/year) owing to basal melting by warm seawater in summer and an increasing relative velocity in winter 2018. The longitudinal stretching could also contribute to the decrease in freeboard. Considering the increase in snow depth, and assuming that the maximum radar return measured by CryoSat-2 is from the snow surface on the iceberg ( $0.82 \pm 0.06$  m/year), the rate of thickness change was estimated to be  $-12.89 \pm 3.34$  m/year between February and November 2018. The volume loss of the iceberg by the ice thinning and calving was approximately  $1.12 \times 10^5$  tons.

These observations reflect the initial evolution of a large tabular iceberg that is unable to drift freely due to surrounding terrain and sea ice. The study demonstrates how Sentinel-1 SAR and CryoSat-2 SIRAL observations can be very useful for investigating the evolution of icebergs. In the near future, iceberg A68A is expected to show much larger-scale changes than have been observed so far. Future study will analyze the influence of such rapid changes on the Antarctic Peninsula marine environment and the flow characteristics of the Larsen C Ice Shelf.

**Author Contributions:** Conceptualization, H.H.; Methodology, H.H.; Formal analysis, H.H., S.L., J.-I.K., S.H.K. and H.-c.K.; Writing—original draft preparation, H.H., S.L., J.-I.K. and S.H.K.; Writing—review and editing, H.H., S.L., J.-I.K. and S.H.K.

**Funding:** This research was funded by the Korea Polar Research Institute (KOPRI), grant number PE18250 and PE19120.

**Conflicts of Interest:** The authors declare no conflict of interest.

## References

1. Silva, T.A.M.; Bigg, G.R.; Nicholls, K.W. Contribution of giant icebergs to the Southern Ocean freshwater flux. *J. Geophys. Res. Oceans* **2006**, *111*, C03004. [[CrossRef](#)]
2. Romanov, Y.A.; Romanova, N.A.; Romanov, P. Shape and size of Antarctic icebergs derived from ship observation data. *Antarct. Sci.* **2011**, *24*, 77–87. [[CrossRef](#)]
3. Tournadre, J.; Bouhier, N.; Girard-Ardhuin, F.; Rémy, F. Antarctic icebergs distributions 1992–2014. *J. Geophys. Res. Oceans* **2016**, *121*, 327–349. [[CrossRef](#)]
4. Martin, S.; Drucker, R.S.; Kwok, R. The areas and ice production of the western and central Ross Sea polynyas, 1992–2002, and their relation to the B-15 and C-19 iceberg events of 2000 and 2002. *J. Mar. Syst.* **2007**, *68*, 201–214. [[CrossRef](#)]
5. Merino, N.; Le Sommer, J.; Durand, G.; Jourdain, N.C.; Madec, G.; Mathiot, P.; Tournadre, J. Antarctic icebergs melt over the Southern Ocean: Climatology and impact on sea ice. *Ocean Model.* **2016**, *104*, 99–110. [[CrossRef](#)]
6. Robinson, N.J.; Williams, M.J.M. Iceberg-induced changes to polynya operation and regional oceanography in the southern Ross Sea, Antarctica, from in situ observations. *Antarct. Sci.* **2012**, *24*, 514–526. [[CrossRef](#)]

7. Wilson, K.; Turney, C.S.M.; Fogwill, C.J.; Blair, E. The impact of the giant iceberg B09B on population size and breeding success of Adélie penguins in Commonwealth Bay, Antarctica. *Antarct. Sci.* **2016**, *28*, 187–193. [[CrossRef](#)]
8. Kooyman, G.L.; Ainley, D.G.; Ballard, G.; Ponganis, P.J. Effects of giant icebergs on two emperor penguin colonies in the Ross Sea, Antarctica. *Antarct. Sci.* **2007**, *19*, 31–38. [[CrossRef](#)]
9. Schwarz, J.N.; Schodlok, M.P. Impact of drifting icebergs on surface phytoplankton biomass in the Southern Ocean: Ocean colour remote sensing and in situ iceberg tracking. *Deep Sea Res. Part I Oceanogr. Res. Pap.* **2009**, *56*, 1727–1741. [[CrossRef](#)]
10. Lasserre, F. Simulations of shipping along Arctic routes: Comparison, analysis and economic perspectives. *Polar Rec.* **2015**, *51*, 239–259. [[CrossRef](#)]
11. Scambos, T.; Ross, R.; Bauer, R.; Yermolin, Y.; Skvarca, P.; Long, D.; Bohlander, J.; Haran, T. Calving and ice-shelf break-up processes investigated by proxy: Antarctic tabular iceberg evolution during northward drift. *J. Glaciol.* **2008**, *54*, 579–591. [[CrossRef](#)]
12. Budge, J.S.; Long, D.G. A comprehensive database for Antarctic iceberg tracking using scatterometer data. *IEEE J. Sel. Top. Appl. Earth Obs. Remote Sens.* **2018**, *11*, 434–442. [[CrossRef](#)]
13. Stuart, K.M.; Long, D.G. Tracking large tabular icebergs using the SeaWinds Ku-band microwave scatterometer. *Deep Sea Res. Part II Top. Stud. Oceanogr.* **2011**, *58*, 1285–1300. [[CrossRef](#)]
14. Wesche, C.; Dierking, W. Near-coastal circum-Antarctic iceberg size distributions determined from Synthetic Aperture Radar images. *Remote Sens. Environ.* **2015**, *156*, 561–569. [[CrossRef](#)]
15. Mazur, A.K.; Wählin, A.K.; Krężel, A. An object-based SAR image iceberg detection algorithm applied to the Amundsen Sea. *Remote Sens. Environ.* **2017**, *189*, 67–83. [[CrossRef](#)]
16. Moctezuma-Flores, M.; Parmiggiani, F. Tracking of the iceberg created by the Nansen Ice Shelf collapse. *Int. J. Remote Sens.* **2017**, *38*, 1224–1234. [[CrossRef](#)]
17. Li, T.; Shokr, M.; Liu, Y.; Cheng, X.; Li, T.; Wang, F.; Hui, F. Monitoring the tabular icebergs C28A and C28B calved from the Mertz Ice Tongue using radar remote sensing data. *Remote Sens. Environ.* **2018**, *216*, 615–625. [[CrossRef](#)]
18. Parmiggiani, F.; Moctezuma-Flores, M.; Guerrieri, L.; Battagliere, M.L. SAR analysis of the Larsen-C A-68 iceberg displacements. *Int. J. Remote Sens.* **2018**, *39*, 5850–5858. [[CrossRef](#)]
19. Wang, F.; Bamber, J.L.; Cheng, X. Accuracy and performance of CryoSat-2 SARIn mode data over Antarctica. *IEEE Geosci. Remote Sens. Lett.* **2015**, *12*, 1516–1520. [[CrossRef](#)]
20. Benn, D.I.; Åström, J.A. Calving glaciers and ice shelves. *Adv. Phys. X* **2018**, *3*, 1513819. [[CrossRef](#)]
21. Jansen, D.; Luckman, A.J.; Cook, A.; Bevan, S.; Kulesa, B.; Hubbard, B.; Holland, P.R. Brief Communication: Newly developing rift in Larsen C Ice Shelf presents significant risk to stability. *Cryosphere* **2015**, *9*, 1223–1227. [[CrossRef](#)]
22. Hogg, A.E.; Gudmundsson, G.H. Impacts of the Larsen-C Ice Shelf calving event. *Nat. Clim. Chang.* **2017**, *7*, 540–542. [[CrossRef](#)]
23. Mueller, R.D.; Padman, L.; Dinniman, M.S.; Erofeeva, S.Y.; Fricker, H.A.; King, M.A. Impact of tide-topography interactions on basal melting of Larsen C Ice Shelf, Antarctica. *J. Geophys. Res. Oceans* **2012**, *117*, C05005. [[CrossRef](#)]
24. Torres, R.; Snoeij, P.; Geudtner, D.; Bibby, D.; Davidson, M.; Attema, E.; Potin, P.; Rommen, B.; Floury, N.; Brown, M.; et al. GMES Sentinel-1 mission. *Remote Sens. Environ.* **2012**, *120*, 9–24. [[CrossRef](#)]
25. Chuter, S.J.; Bamber, J.L. Antarctic ice shelf thickness from CryoSat-2 radar altimetry. *Geophys. Res. Lett.* **2015**, *42*, 10721–10729. [[CrossRef](#)]
26. Helm, V.; Humbert, A.; Miller, H. Elevation and elevation change of Greenland and Antarctica derived from CryoSat-2. *Cryosphere* **2014**, *8*, 1539–1559. [[CrossRef](#)]
27. Förste, C.; Bruinsma, S.; Abrikosov, O.; Flechtner, F.; Marty, J.C.; Lemoine, J.-M.; Dahle, C.; Numayer, H.; Barthellmes, F.; König, R.; et al. EIGEN-6C4—The latest combined global gravity field model including GOCE data up to degree and order 1949 of GFZ Potsdam and GRGS Toulouse. In Proceedings of the EGU General Assembly Conference Abstract, Vienna, Austria, 27 April–2 May 2014; Volume 16.
28. Knudsen, P.; Andersen, O.B. A global mean ocean circulation estimation using GOCE gravity models—The DTU12MDT mean dynamic topography model. In *20 Years of Progress in Radar Altimetry Abstract Book*; European Space Agency: Paris, France, 2012; p. 123.

29. Padman, L.; Erofeeva, S.Y.; Fricker, H.A. Improving Antarctic tide models by assimilation of ICESat laser altimetry over ice shelves. *Geophys. Res. Lett.* **2008**, *35*, L22504. [[CrossRef](#)]
30. Gelaro, R.; McCarty, W.; Suárez, M.J.; Todling, R.; Molod, A.; Takacs, L.; Randles, C.A.; Darmenov, A.; Bosilovich, M.G.; Reckle, R.; et al. The modern-era retrospective analysis for research and applications, version 2 (MERRA-2). *J. Clim.* **2017**, *30*, 5419–5454. [[CrossRef](#)]
31. Fretwell, P.; Pritchard, H.D.; Vaughan, D.G.; Bamber, J.L.; Barrand, N.E.; Bell, R.; Bianchi, C.; Bingham, R.G.; Blankenship, D.D.; Casassa, G.; et al. Bedmap2: Improved ice bed, surface and thickness datasets for Antarctica. *Cryosphere* **2013**, *7*, 375–393. [[CrossRef](#)]
32. Silva, T.A.M.; Bigg, G.R. Computer-based identification and tracking of Antarctic icebergs in SAR images. *Remote Sens. Environ.* **2005**, *94*, 287–297. [[CrossRef](#)]
33. Ford, M. Shoreline changes interpreted from multi-temporal aerial photographs and high resolution satellite images: Wotje Atoll, Marshall Island. *Remote Sens. Environ.* **2013**, *135*, 130–140. [[CrossRef](#)]
34. Zwally, H.J.; Yi, D.; Kwok, R.; Zhao, Y. ICESat measurements of sea ice freeboard and estimates of sea ice thickness in the Weddell Sea. *J. Geophys. Res. Oceans* **2008**, *113*, C02S15. [[CrossRef](#)]
35. Griggs, J.A.; Bamber, J.L. Ice shelf thickness over Larsen C, Antarctica, derived from satellite altimetry. *Geophys. Res. Lett.* **2009**, *36*, L19501. [[CrossRef](#)]
36. Griggs, J.A.; Bamber, J.L. Antarctic ice-shelf thickness from satellite radar altimetry. *J. Glaciol.* **2011**, *57*, 485–498. [[CrossRef](#)]
37. Paolo, F.S.; Fricker, H.A.; Padman, L. Volume loss from Antarctic ice shelves is accelerating. *Science* **2015**, *348*, 327–331. [[CrossRef](#)] [[PubMed](#)]
38. Han, H.; Lee, H. Tide-corrected flow velocity and mass balance of Campbell Glacier Tongue, East Antarctica, derived from interferometric SAR. *Remote Sens. Environ.* **2015**, *160*, 180–192. [[CrossRef](#)]
39. Zwally, H.J.; Giovinetto, M.B.; Li, J.; Cornejo, H.G.; Beckley, M.A.; Brenner, A.C.; Saba, J.L.; Yi, D. Mass changes of the Greenland and Antarctic ice sheets shelves and contributions to sea-level rise: 1992–2002. *Ann. Glaciol.* **2005**, *51*, 509–527. [[CrossRef](#)]
40. Wagner, T.J.W.; Wadhams, P.; Bates, R.; Elosegui, P.; Stern, A.; Vella, D.; Povl Abrahamsen, E.; Crawford, A.; Nicholls, K.W. The “footloose” mechanism: Iceberg decay from hydrostatic stresses. *Geophys. Res. Lett.* **2014**, *41*, 5522–5529. [[CrossRef](#)]
41. Liu, H.; Li, X.; Guo, H. The dynamic processes of sea ice on the east coast of Antarctica—A case study based on spaceborne synthetic aperture radar data from TerraSAR-X. *IEEE J. Sel. Top. Appl. Earth Obs. Remote Sens.* **2016**, *9*, 1187–1198. [[CrossRef](#)]
42. Thomas, R.H. The dynamics of marine ice sheets. *J. Glaciol.* **1979**, *24*, 167–177. [[CrossRef](#)]
43. Walter, F.; O’Neel, S.; McNamara, D.; Pfeffer, W.T.; Bassis, J.N.; Fricker, H.A. Iceberg calving during transition from grounded to floating ice: Columbia Glacier, Alaska. *Geophys. Res. Lett.* **2010**, *37*, L15501. [[CrossRef](#)]
44. Ren, D.; Leslie, L.M.; Lynch, M.J. Verification of model simulated mass balance, flow fields and tabular calving events of the Antarctic ice sheet against remotely sensed observations. *Clim. Dyn.* **2013**, *40*, 2617–2636. [[CrossRef](#)]
45. Jansen, D.; Schodlok, M.; Rack, W. Basal melting of A-38B: A physical model constrained by satellite observations. *Remote Sens. Environ.* **2007**, *111*, 195–203. [[CrossRef](#)]
46. Stephenson, G.R., Jr.; Sprintall, J.; Gille, S.T.; Vernet, M.; Helly, J.J.; Kaufmann, R.S. Subsurface melting of a free-floating Antarctic iceberg. *Deep Sea Res. Part II Top. Stud. Oceanogr.* **2011**, *58*, 1336–1345. [[CrossRef](#)]

